CORRECTING THE VARIATIONS OF BOLD SIGNAL DUE TO SUSCEPTIBILITY-INDUCED MAGNETIC FIELD GRADIENTS AND ITS APPLICATION

BY

DAVID J. HO

THESIS

Submitted in partial fulfillment of the requirements
for the degree of Master of Science in Electrical and Computer Engineering
in the Graduate College of the
University of Illinois at Urbana-Champaign, 2012

Urbana, Illinois

Adviser:

Assistant Professor Brad Sutton

ABSTRACT

Functional magnetic resonance imaging (fMRI) using blood oxygenation level dependent (BOLD) signals is a tool that is currently used in many cognitive neuroscience studies. However, many studies do not consider susceptibility-induced magnetic field gradients. Susceptibility-induced magnetic field gradients can vary echo time, which can also vary BOLD sensitivity. In order to correct artifacts, we introduce percent signal change and calibration function. We show calibration can reduce the artifacts and can be applied in many studies such as age-related studies.

I love you, O LORD, my strength.

ACKNOWLEDGMENTS

This master's thesis could not have been written without Assistant Professor Brad Sutton, who not only has helped me to finish this research but has also encouraged and challenged me in many different ways throughout my academic program. Thank you.

I also want to acknowledge my colleagues, Maojing Fu, Joe Holtrop, Jiading Gai, Thomas Paine, Cheng Ouyang, and Andrew Naber.

I also want to acknowledge my family who has been supporting me to study in America.

Lastly, I want to thank God who has been guiding my life. It is all possible because of His love.

TABLE OF CONTENTS

CHAPTER 1

INTRODUCTION

Functional magnetic resonance imaging (fMRI), using blood oxygenation level dependent (BOLD) signals, is the most pervasive tool in cognitive neuroscience to non-invasively examine which parts of the brain are involved in which functions and to look at changes in function across the lifespan. This technique relies on changes in the magnetic susceptibility of blood, which depends on the oxygenation state of hemoglobin. fMRI is sensitive to the microscopic magnetic susceptibility variations in blood. For example, as neuronal activity provokes an increase in oxygen consumption and blood flow, the number of oxygenated hemoglobin will increase and the number of deoxygenated hemoglobin will decrease in that region, and MRI can detect the change in the T_2^*-weighted signal.

Beyond the microscopic magnetic susceptibility variations, the macroscopic magnetic susceptibility variations can affect signals in fMRI. For example, there is a large magnetic susceptibility difference from air/tissue interfaces, which leads to severe disruptions of the uniformity of the magnetic field around that area. The susceptibility-induced magnetic field inhomogeneity causes image distortion and signal loss. There have been many studies to develop and optimize correcting susceptibility magnetic field inhomogeneity artifacts of image distortion and signal loss [1, 2, 3, 4].

The effect of gradients in the magnetic field due to macroscopic field inhomogeneity can cause additional artifacts for gradient-echo based functional MRI. Echo time is defined as the time point when the origin or the center of k-space is sampled. The effective echo time from a distorted k-space trajectory caused by susceptibility-induced magnetic field gradients will be different from the nominal echo time. Since the BOLD signal is a function of the echo time of the acquisition, susceptibility-induced magnetic field gradients can result in a spatially varying BOLD signal.

In this research, we are going to focus on correcting the variations of BOLD

signals due to echo time changes caused by susceptibility-induced magnetic field gradients. First of all, we are going to observe how magnetic susceptibility differences can disrupt the BOLD sensitivity and correct this effect by calibration. Also, we are going to address how magnetic susceptibility differences across groups in a study of brain differences can result in identifying differences that are not due to underlying brain activity differences, such as in aging studies.

CHAPTER 2

BACKGROUND

2.1 Magnetic Resonance Imaging

Magnetic resonance imaging (MRI) is one of the tomography techniques to create an internal image non-invasively by using radio frequency (RF) pulses. In order to understand the physics behind MRI, we need to understand nuclear magnetic resonance (NMR). Nuclei having odd numbers of neutrons, protons, or both, such as in hydrogen atoms, possess an angular momentum, $\overrightarrow{J}$, which is also called spin. Nuclei having spin create a magnetic field, $\overrightarrow{\mu}$, which is also called a magnetic moment. The relationship between the angular momentum and the magnetic moment is

$$\overrightarrow{\mu} = \gamma \overrightarrow{J} \tag{2.1}$$

where γ is called the gyromagnetic ratio. $\bar{\gamma}$ is also widely used where

$$\bar{\gamma} = \frac{\gamma}{2\pi} \tag{2.2}$$

Gyromagnetic ratio is nucleus-dependent. For example, $\bar{\gamma} = 42.58$ MHz/T for ^1H while $\bar{\gamma} = 11.26$ MHz/T for ^{31}P.

A net magnetization, $\overrightarrow{M}$, is defined as the sum of all magnetic moments.

$$\overrightarrow{M} = \sum_{n=1}^{N_s} \overrightarrow{\mu_n} \tag{2.3}$$

where N_s is the total number of spins in the object being imaged. If there is no magnetic field, all magnetic moments will have random directions and the net magnetization will be zero.

In order to receive signals from the magnetization, we use a static magnetic

field and a radio frequency pulse. A static magnetic field, also called B_0-field, or $\overrightarrow{B_0}$, is a field that is strong and uniform. A radio frequency (RF) pulse, also called B_1-field, or $\overrightarrow{B_1}$, is a field that is weak and short. Usually $\overrightarrow{B_1}$ is turned on for a few microseconds or milliseconds with a weak magnetic field such as $B_1 = 50$ mT while $B_0 = 1.5$ T [5].

If there is $\overrightarrow{B_0}$, then magnetic moments will be aligned to the magnetic field, either parallel or anti-parallel. If B_1-field is applied, the spins that have the same frequency as the RF pulse will become excited by absorbing energy and tip down from the direction of B_0. This process is called excitation. When the net magnetization is tipped down, it precesses around the magnetic field with the Larmor frequency.

$$\omega_0 = \gamma B_0 \tag{2.4}$$

where B_0 is the magnitude of the static magnetic field. Note that because of the existence of inhomogeneities in the B_0-field and the chemical shift effect, a specific spin system may have a range of resonance frequencies and each set of spins at a certain frequency is called an isochromat [5].

The flip angle, α, is determined by the strength, B_1, and the duration, τ_p, of RF pulse.

$$\alpha = \int_0^{\tau_p} \gamma B_1(t) dt \tag{2.5}$$

After the short RF pulse, the net magnetization will slowly recover to its equilibrium. This process is called relaxation. As the net magnetization recovers to the static magnetic field direction, the longitudinal magnetization will be recovered, which is called longitudinal relaxation, and the transverse magnetization will be decayed, which is called transverse relaxation. The recovery rate of the longitudinal magnetization is characterized by the time constant T_1; after time T_1, the longitudinal magnetization has returned to 63% of its final value. The decay rate of the transverse magnetization is characterized by the time constant T_2; after time T_2, the transverse magnetization has lost 63% of its original value. If the magnetic field is inhomogeneous, the transverse magnetization will decay faster because magnetic moments can cancel out each other with a small magnetic field differences and the time constant is called T_2^*.

Figure 2.1 shows relaxation curves both in longitudinal axis and transverse plane. This figure shows that $T_1 > T_2 > T_2^*$.

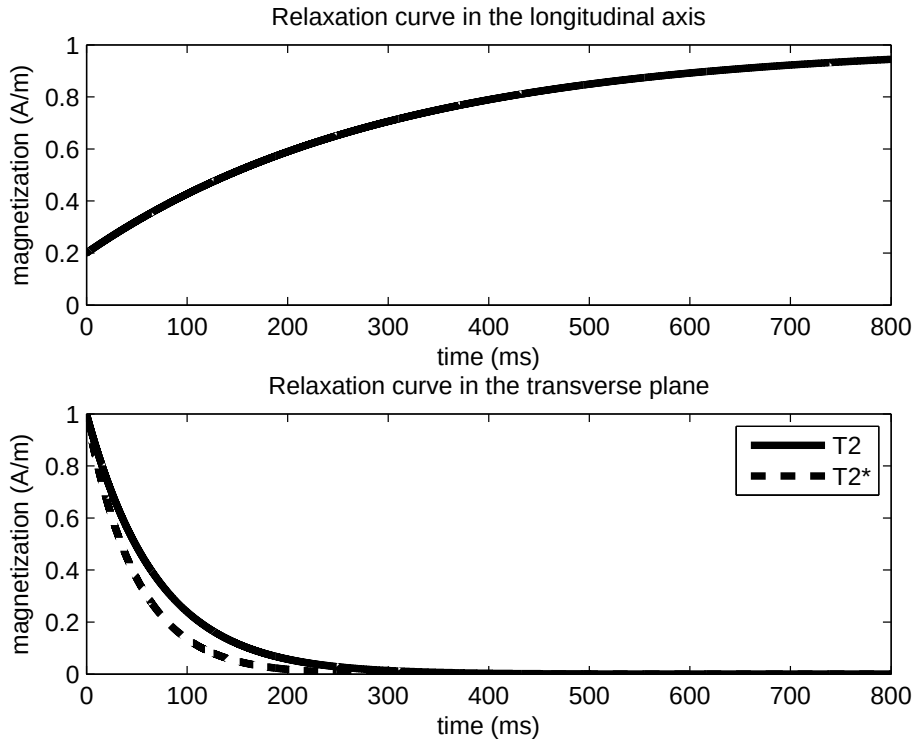

Figure 2.1: Relaxation curve in the longitudinal axis and relaxation curve in the transverse axis. In this figure, the parameters are the following: $T_1 = 300$ ms, $T_2 = 70$ ms, and $T_2^* = 50$ ms.

2.2 Functional MRI

Functional MRI (fMRI) detects the signal changes due to neural activities in a brain. If one area in a brain is active, there will be more oxygenated hemoglobin and less deoxygenated hemoglobin. If the area is not active, there will be less oxygenated hemoglobin and more deoxygenated hemoglobin. Fully oxygenated hemoglobin is slightly diamagnetic and deoxygenated hemoglobin is paramagnetic. The deoxygenated hemoglobin distorts the static magnetic field less during neural activity. The MRI signal will decay more if there are more deoxygenated hemoglobin molecules because of rapid phase cancellation and it will change the MR decay parameter, T_2^*. If the region is not active and there are more deoxygenated hemoglobin molecules, then the signal is low. However, if the region is active and there are less deoxygenated hemoglobin molecules, then the signal is high. Figure 2.2 shows that high signals mean the region is active and low signals mean the region is inactive. Therefore, if a T_2^*-weighted image is measured, we are

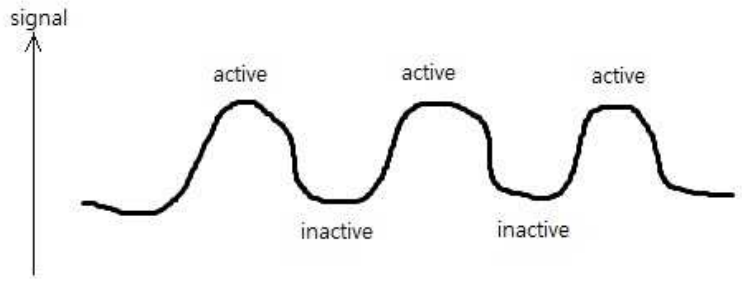

Figure 2.2: If the BOLD signal is high, it means the region is active. If the BOLD signal is low, it means the region is inactive.

able to find which regions are active and which regions are not active. This technique is called blood oxygenation level dependent (BOLD) contrast.

fMRI is performed by acquiring a time series of snapshot images of the brain, typically every two seconds for several minutes. During this time, subjects are presented with visual-based or other stimuli that change throughout the scan. Examining how the measured brain signal correlates with the presented stimuli will reveal which areas of the brain are undergoing activity and associated changes in the concentration of deoxygenated hemoglobin.

2.3 K-Space Trajectories

K-space is where the signals are recorded. Signals in k-space, $S\left(\overrightarrow{k}\right)$, are the Fourier transform of a spatial function, $\rho\left(\overrightarrow{r}\right)$.

$$S\left(\overrightarrow{k}\right) = \mathcal{F}\{\rho\left(\overrightarrow{r}\right)\} = \int_{-\infty}^{\infty} \cdots \int_{-\infty}^{\infty} \rho\left(\overrightarrow{r}\right) e^{-i2\pi \overrightarrow{k} \cdot \overrightarrow{r}} d\overrightarrow{r} \tag{2.6}$$

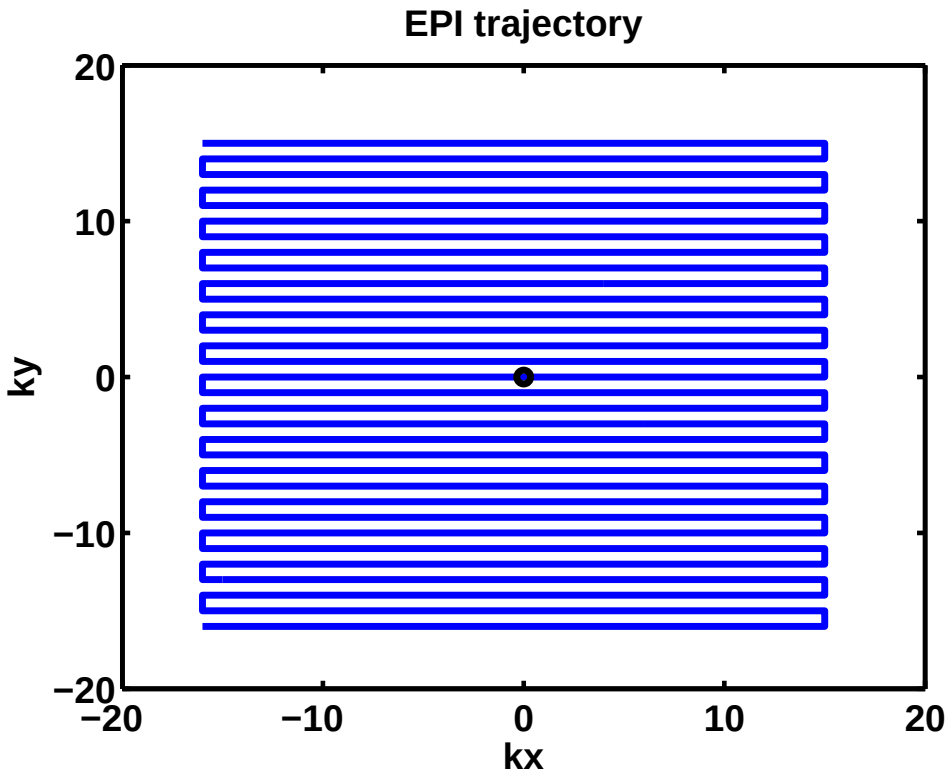

Figure 2.3: EPI trajectory with FOV = 24 cm, reconstruction size = 32. This is a unitless k-space trajectory which is $k_x \times FOV_x$.

In the same way, in order to reconstruct the spatial image from the signals in k-space, the inverse Fourier transform can be

$$\rho\left(\overrightarrow{r}\right) = \mathcal{F}\{S\left(\overrightarrow{k}\right)\} = \int_{-\infty}^{\infty} \cdots \int_{-\infty}^{\infty} S\left(\overrightarrow{k}\right) e^{i2\pi \overrightarrow{k} \cdot \overrightarrow{r}} d\overrightarrow{k} \tag{2.7}$$

Location in k-space is decided by the integration of gradients.

$$\overrightarrow{k}\left(t\right) = \bar{\gamma} \int_{0}^{t} \overrightarrow{G}\left(\tau\right) d\tau \tag{2.8}$$

There are many ways to traverse k-space with different trajectories. The two most popular trajectories will be introduced in this section. The first trajectory is the echo-planar imaging (EPI) trajectory [5, 6]. The trajectory starts from a corner of k-space and it only moves in the y-direction once it reaches the border of k-space in the x-direction.

Figure 2.3 shows the EPI trajectory. EPI can sample all k-space uniformly as shown in Figure 2.3. However, EPI is not the time-efficient method, because the slew rate from the changes of the x-direction and the y-direction

will slow down the sampling rate. Slew rate, S_R, is a rate of change of gradient field and the unit is teslas per meter per second [6].

When EPI is performed, there are two ways you can sample, EPI-down and EPI-up. EPI-down, also called phase-encode anterior to posterior (PEAP), starts the trajectory from the top of the k-space to the bottom. EPI-up, also called phase-encode posterior to anterior (PEPA), starts the trajectory from the bottom of the k-space to the top. The direction of sampling can be an issue when the inhomogeneity of magnetic fields is considered.

By the sampling theorem,

$$\Delta k_x \leq \frac{1}{FOV_x} \tag{2.9}$$

$$\Delta k_y \leq \frac{1}{FOV_y} \tag{2.10}$$

where FOV_x and FOV_y are the field of view in the x-direction and the y-direction, respectively. Also, Δk_x and Δk_y are the sample spacing in the x-direction and the y-direction, respectively. If these sampling requirements are not satisfied, then there will be aliasing.

Another trajectory is the spiral trajectory [5, 6, 7].

Figure 2.4 shows the spiral trajectory. According to Liang, a spiral trajectory can be described mathematically as following:

$$\overrightarrow{k}(t) = A\omega(t)\, e^{i\omega(t)} \tag{2.11}$$

where $\overrightarrow{k} = k_x + ik_y$ and ω is a function of time [5]. Since a spiral trajectory does not have any sudden changes, it will not be as slow as an EPI trajectory. However, a spiral trajectory cannot collect the data on the corners of k-space, as you can see Figure 2.4 [6].

There are also two ways the trajectory can be sampled. Spiral-out is a trajectory that samples from inside of the k-space, the origin of the k-space, to outside of the k-space. Spiral-in is a trajectory that samples from outside of the k-space to inside of the k-space. Since echo time is defined as the time when the k-space trajectory crosses the center of the k-space, echo time of an ideal spiral-out occurs at the beginning of the readout and echo time of the spiral-in trajectory occurs at the end of the readout, limiting the minimum echo time achieveable.

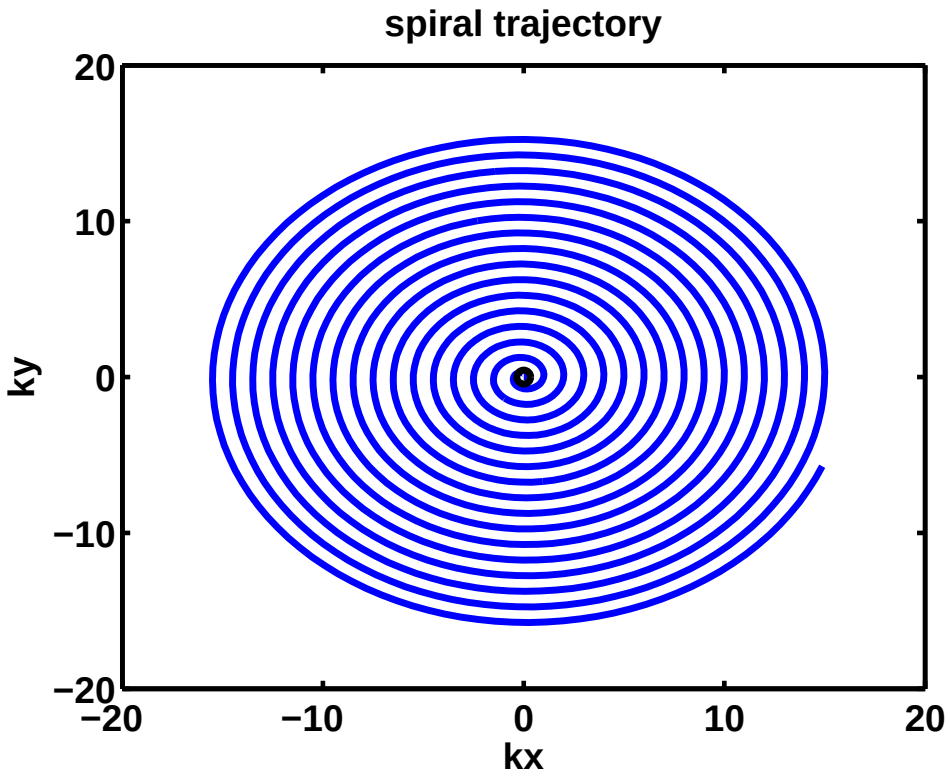

Figure 2.4: Spiral trajectory with FOV = 24cm, reconstruction size = 32. This is a unitless k-space trajectory which is $k_x \times FOV_x$.

By the sampling theorem,

$$\Delta k_{rad} \leq \frac{1}{FOV_{rad}} \tag{2.12}$$

where FOV_{rad} is the size of the circular field of view in the radial-direction.

2.4 Magnetic Susceptibility

Magnetic susceptibility, χ_m, is defined by the relationship between the magnetic field, $\overrightarrow{B}$, and the magnetization, $\overrightarrow{M}$.

$$\overrightarrow{B} = \frac{1+\chi_m}{\chi_m}\mu_0\overrightarrow{M} \tag{2.13}$$

where μ_0 the permeability of free space. The quantity, χ_m, which is a dimensionless parameter, is a measure of the degree of magnetizability of the material [8].

Magnetic susceptibility can vary between different materials ($\chi_{tissue} = -9 \times 10^{-6}$ and $\chi_{air} = 0.4 \times 10^{-6}$) [3] and cause variations of the magnetic field which leads to image artifacts such as geometric distortion and phase effects. A susceptibility-induced magnetic field gradient is defined as a gradient that is caused by different susceptibilities between different materials. For example, Truong et al. found magnetic field and gradient inhomogeneities near air/tissue interfaces which are caused by the susceptibility differences between air and tissue [3]. The susceptibility-induced magnetic field gradients result from distributions of the magnetic field across the sample to be imaged.

Variations of magnetic susceptibility cause variations of magnetic field according to Equation 2.13 and variations of magnetic field cause image artifacts such as geometric distortion and phase effects [9]. The phase variation due to the magnetic field variation at location, $\overrightarrow{r}$, in a given echo time, T_E, can be expressed as

$$\phi(\overrightarrow{r}, T_E) = \phi_0 - \gamma \Delta B(\overrightarrow{r}) T_E \tag{2.14}$$

where ϕ_0 is a constant phase offset independent of time and $\Delta B(\overrightarrow{r})$ is the presence of local variations in the magnetic field. By scanning with different echo times, T_{E_1} and T_{E_2}, we can extract the magnetic field inhomogeneity as a spatial map.

$$\Delta B(\overrightarrow{r}) = \frac{\phi(\overrightarrow{r}, T_{E_2}) - \phi(\overrightarrow{r}, T_{E_1})}{\gamma(T_{E_1} - T_{E_2})} \tag{2.15}$$

2.5 Signal Equation with Field Inhomogeneity

As we define in Equation 2.6, the signal equation is

$$S\left(\overrightarrow{k}\right) = \int_{-\infty}^{\infty} \cdots \int_{-\infty}^{\infty} \rho\left(\overrightarrow{r}\right) e^{-i2\pi \overrightarrow{k} \cdot \overrightarrow{r}} d\overrightarrow{r} \tag{2.16}$$

where ρ is the spatial function. Equation 2.16 is an ideal Fourier transform between the spatial function and the k-space data. By this equation, the image can be reconstructed from the k-space data. However, there is an assumption in Equation 2.16; that is, the static magnetic field has to be

homogeneous. This assumption is not true in reality. For example, different susceptibilities can cause an inhomogeneity. If inhomogeneity terms are added, Equation 2.16 will be generalized to

$$S\left(\overrightarrow{k}\right) = \int_{-\infty}^{\infty} \cdots \int_{-\infty}^{\infty} \rho\left(\overrightarrow{r}\right) e^{-i2\pi \overrightarrow{k} \cdot \overrightarrow{r}} e^{-it\omega(\overrightarrow{r})} d\overrightarrow{r} \tag{2.17}$$

where $\omega(\overrightarrow{r})$ is the multiplication of the field inhomogeneity with γ. ω is the off-resonant frequency that results from the field inhomogeneity. Without accounting for the field inhomogeneity term, we will not get an accurate image reconstruction. However, if we account for it, we can correct the distortions. Although an MRI scanner has shim coils to help make the magnetic field more uniform across a sample, field inhomogeneity still exists when an object is placed inside the large magnetic field.

CHAPTER 3

SUSCEPTIBILITY-INDUCED BOLD SIGNAL CHANGE

3.1 Motivation

3.1.1 The Effect of Susceptibility-Induced Magnetic Field Gradients

As shown in Equation 2.8, the location in k-space at which we are sampling is determined by the imaging gradients as

$$\overrightarrow{K}_{imaging}(t) = \bar{\gamma} \int_0^t \overrightarrow{G}_{imaging}(\tau)\, d\tau \tag{3.1}$$

However, field inhomogeneity across a sample caused by susceptibility leads to gradients, $\overrightarrow{G}_{susc}$, in the magnetic field which vary across the sample. For a particular voxel, we have a gradient in the magnetic field. If the field inhomogeneity is $w(x, y)$, we can linearly expand that at a voxel as:

$$w(x,y) = w(x_0,y_0) + G_{susc,x}(x_0,y_0) \times (x - x_0) + G_{susc,y}(x_0,y_0) \times (y - y_0) \tag{3.2}$$

Then the location in k-space generated by susceptibility-induced magnetic field gradients alone is

$$\overrightarrow{K}_{susc}(t) = \bar{\gamma}\overrightarrow{G}_{susc}(t + t_0) \tag{3.3}$$

where $\overrightarrow{G}_{susc}$ is a constant that is a vector consisting of the x- and y- gradient components and is a function of spatial position in the object to be imaged, and t_0 is the duration between the RF pulse and the beginning of the data acquisition. In this case, $t = 0$ when the data acquisition starts.

As Equation 3.1 and Equation 3.3 are combined, the location in k-space

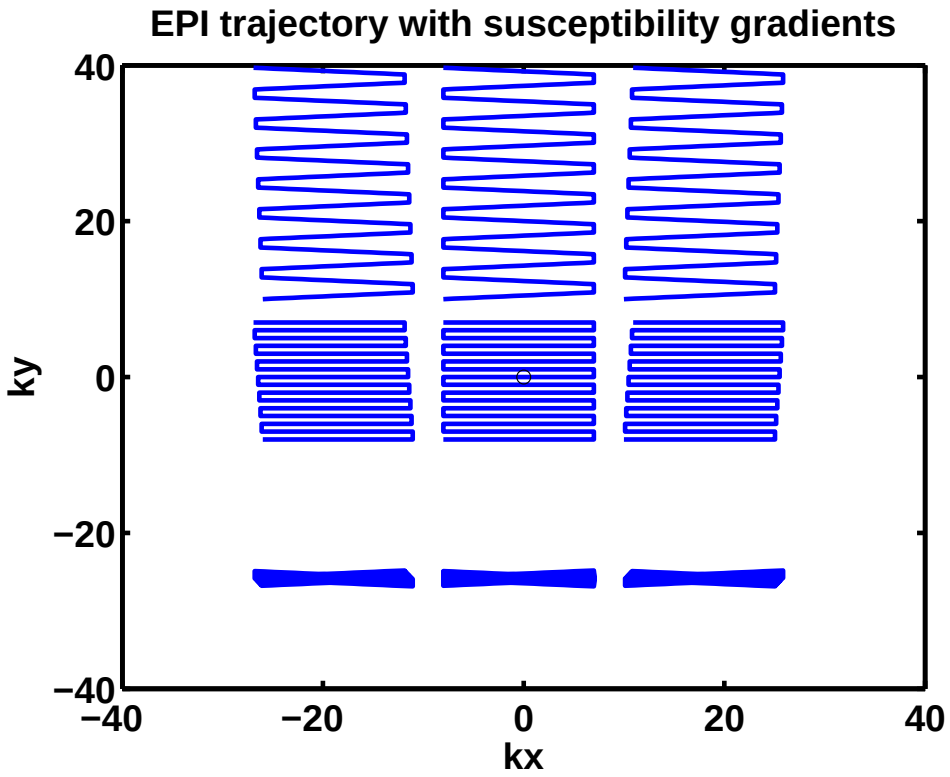

Figure 3.1: EPI trajectory with susceptibility gradients. In this plot, FOV = 24 cm, and setup timing of slice acquisition = 5 μs, G_{susc} = 30 T/m applied in each direction x and y and in both.

generated by imaging gradients with susceptibility is

$$\overrightarrow{K}(t) = \bar{\gamma} \int_0^t \overrightarrow{G}_{imaging}(\tau)\, d\tau + \bar{\gamma}\overrightarrow{G}_{susc}(t + t_0) \tag{3.4}$$

Figure 3.1 and Figure 3.2 show how trajectories can be shifted and skewed by susceptibility gradients.

Since echo time is defined as the time when the k-space trajectory passes the center of the k-space, the shifted and skewed trajectory and the direction by which the k-space trajectory is traversed will change the echo time. For example, assume the susceptibility gradient is applied in the y-direction. Then the k-space trajectory will be shifted and skewed upward. If the trajectory is EPI-up, susceptibility gradients will act with the imaging gradients to reach the center of k-space early in the readout and the echo time will be shorter than the original echo time. If the trajectory is skewed and shifted too much, then it may not pass the center of the k-space anymore and we cannot find the echo time in that case.

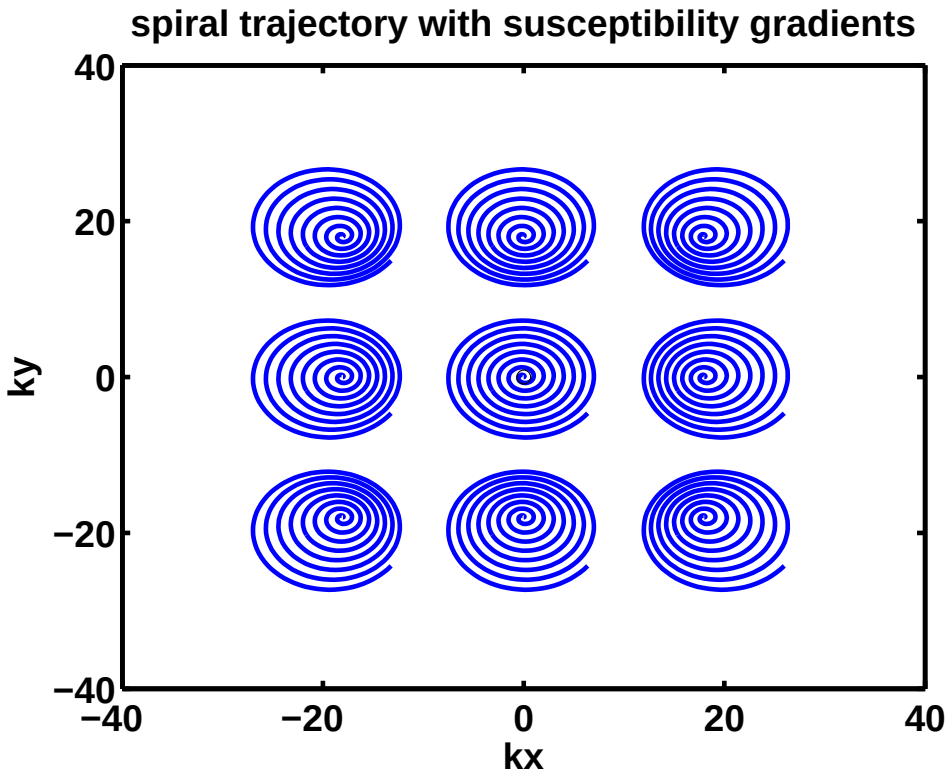

Figure 3.2: Spiral trajectory with susceptibility gradients. In this plot, FOV = 24 cm, and setup timing of slice acquisition = 5 μs, G_{susc} = 30 T/m applied in each direction x and y and in both.

According to [2], changes in echo time will lead to changes in BOLD sensitivity. To reduce BOLD sensitivity changes, there have been several studies in the past. Deichmann et al. suggested adjusting the slice prescription tilt angle and using gradient precompensation in the slice direction [10]. De Panfilis and Schwarzbauer optimized the slice angle and the compensation gradient along with the phase encoding direction for EPI [11]. Weiskopf et al. determined maps for the optimal parameters of slice tilt, phase encoding direction, and z-shimming [12]. In the follow-up paper, they studied the importance of correcting susceptibility-induced gradients in the readout direction and reduced signal loss by decreasing echo time and increasing spatial resolution in the readout direction [13]. Balteau et al. introduced the BOLD-sensitivity-based shimming technique to improve sensitivity in a target region through a targeted shimming process while not significantly degrading the BOLD sensitivity in other regions [14]. In following sections, percent signal change and calibration function will be introduced to reduce the artifacts.

3.1.2 Percent Signal Change

Percent signal change is a technique that is commonly used in fMRI to compare activations between groups to determine functionally relevant changes in specified regions of interest. Cohen and DuBois showed that percent signal change as an outcome measure for an fMRI study is robust and stable across trials within the same subject and across subjects compared to examining thresholded activation maps [15]. Chee et al. demonstrated that percent signal change measures in fMRI show less intersession variability than examining and analyzing thresholded activation maps [16].

Percent signal change (PSC) is defined as

$$PSC(TE) = \frac{s_0\left(e^{-\frac{TE}{T^*_{2,active}}} - e^{-\frac{TE}{T^*_{2,rest}}}\right)}{s_0 e^{-\frac{TE}{T^*_{2,rest}}}} \times 100 \tag{3.5}$$

where TE is an echo time, s_0 is the voxel image intensity without T_2^* relaxation, $T^*_{2,rest}$ is the T_2^* relaxation time constant during resting stage, and $T^*_{2,active}$ is the T_2^* relaxation time constant during active stage. $s_0 e^{-\frac{TE}{T^*_{2,active}}}$ means the fMRI signal received during the task when the tissue is active and $s_0 e^{-\frac{TE}{T^*_{2,rest}}}$ means the fMRI signal received during rest. $T^*_{2,rest} = 48.9$ ms and $T^*_{2,active} = 49.6$ ms are used [17].

If susceptibility-induced magnetic field gradients are added, then the k-space trajectory will be shifted and skewed and the echo time will be changed. Percent signal change with susceptibility gradients can be defined as

$$PSC(TE_{eff}) = \frac{s_0\left(e^{-\frac{TE_{eff}}{T^*_{2,active}}} - e^{-\frac{TE_{eff}}{T^*_{2,rest}}}\right)}{s_0 e^{-\frac{TE_{eff}}{T^*_{2,rest}}}} \times 100 \tag{3.6}$$

where TE_{eff} is the effective echo time which is the echo time after including the effects of the susceptibility gradients.

3.1.3 Calibration Function

Calibration function is defined as the ratio between Equation 3.6 and Equation 3.5, forming the signal change expected from including susceptibility

gradients normalized by the nominal percent signal change in the absence of susceptibility gradients:

$$C(TE_{eff}) = \frac{PSC(TE_{eff})}{PSC(TE)} \tag{3.7}$$

The calibration function implies the scaling of BOLD sensitivity due to the effective echo time caused by susceptibility-induced magnetic field gradients. As we divide the measured percent signal change by $C(TE_{eff})$, we are able to remove the artifacts by susceptibility-induced magnetic field gradients and find the correct percent signal change.

3.1.4 Validation of Calibration

In this subsection, the validity of the calibration process across a range of baseline T_2^* values is examined.

First of all, let us define a variable, α, such as

$$\alpha = \frac{T^*_{2,rest}}{T^*_{2,active}} \tag{3.8}$$

If there is no big activation, α will be close to 1, because $T^*_{2,rest} \approx T^*_{2,active}$. However, if there is a big activation, α will be less than 1, because $T^*_{2,rest} < T^*_{2,active}$.

Let us also define α_0 based on the values from [17]:

$$\alpha_0 = \frac{T^*_{2,rest}}{T^*_{2,active}} = 0.9859 \tag{3.9}$$

where $T^*_{2,rest} = 48.9$ ms and $T^*_{2,active} = 49.6$ ms.

With α, Equation 3.5 and Equation 3.7 can be modified as following:

$$PSC(\alpha, TE) = \left(e^{(1-\alpha)\times\frac{TE}{T^*_{2,rest}}} - 1 \right) \times 100 \tag{3.10}$$

$$C(\alpha, TE_{eff}) = \frac{PSC(\alpha, TE_{eff})}{PSC(\alpha, TE)} = \frac{e^{(1-\alpha)\times\frac{TE_{eff}}{T^*_{2,rest}}} - 1}{e^{(1-\alpha)\times\frac{TE}{T^*_{2,rest}}} - 1} \tag{3.11}$$

From Equation 3.10, α can be expressed as

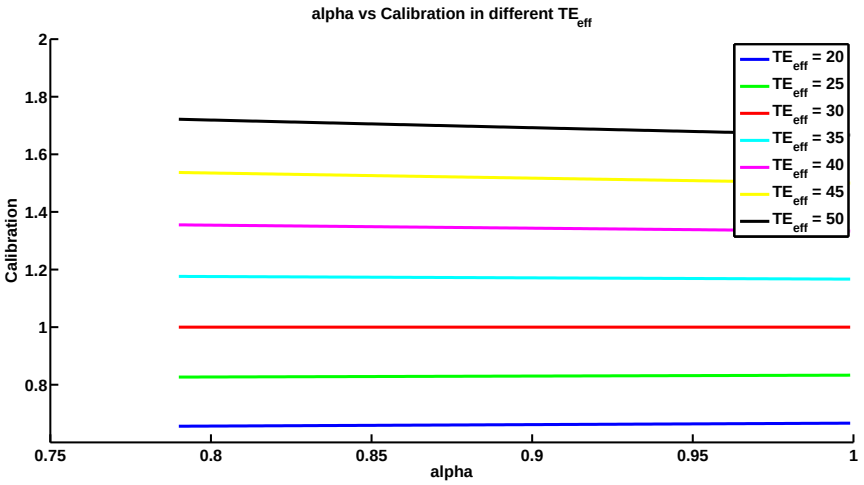

Figure 3.3: α vs calibration in different TE_{eff}.

$$\alpha = 1 - \frac{T^*_{2,rest}}{TE} \ln\left(\frac{PSC}{100} + 1\right) \tag{3.12}$$

Since we are interested in the region of $0 < PSC < 10$, the corresponding region is $0.7903 < \alpha < 1$.

For $\alpha = \alpha_0$, the PSC with the effective echo time can be calculated by

$$PSC(\alpha_0, TE) = \frac{PSC(\alpha_0, TE_{eff})}{C(\alpha_0, TE_{eff})} \tag{3.13}$$

In order to show the validation of calibration, we need to show that the PSC with α and the effective echo time can be calculated by $C(\alpha_0, TE_{eff})$ although $\alpha \neq \alpha_0$.

$$PSC(\alpha, TE) = \frac{PSC(\alpha, TE_{eff})}{C(\alpha_0, TE_{eff})} \tag{3.14}$$

To show Equation 3.14, we plot calibration functions with respect to α in several different TE_{eff}'s in Figure 3.3. Whether $\alpha = \alpha_0$ or not, the calibration values are consistent in the same TE_{eff}'s. The plot implies

$$C(\alpha_0, TE_{eff}) = C(\alpha, TE_{eff}) \quad where \quad \alpha \neq \alpha_0 \tag{3.15}$$

which is equivalent to

$$C(\alpha_0, TE_{eff}) = \frac{PSC(\alpha, TE_{eff})}{PSC(\alpha, TE)} \quad where \quad \alpha \neq \alpha_0 \tag{3.16}$$

which is equivalent to Equation 3.14.

Equation 3.14 is very important, because it means percent signal change from a range of baseline T_2^* values with the echo time can be calculated by percent signal change with the effective echo time and calibration function from a specific T_2^*. Not relying only on mathematics, we are also going to experiment with BOLD signals generated from a breath hold task to show that calibration can correct artifacts from magnetic susceptibility in the following section.

3.2 Procedures

3.2.1 Acquisition Protocol and Participants

Subjects were scanned in accordance with the local institutional review board and subjects properly consented after being informed about the study. Twenty-eight healthy adult subjects participated in the study, including fourteen young adults (19-32 years old, mean age 25, 8 females) and fourteen old adults (61-72 years old, mean age 66, 7 females). Subject scans were performed using a Siemens (Erlangen, Germany) Allegra 3 T MRI scanner. Magnetic field maps were acquired with the vendor-supplied multi-echo gradient echo sequence with the following parameters: TE = 4.89, 7.35 ms, TR = 390 ms, field of view = 24 cm, matrix size = 64x64, 32 slices 4 mm thick, oblique-axial scans aligned to AC-PC.

3.2.2 Breath Hold Task for Global Activation

To examine the effectiveness of our calibration, we used a breath hold task in order to generate a whole brain activation that is similar to the BOLD signal [18]. This is similar to the task used by Deichmann and colleagues previously to investigate BOLD sensitivity changes [2]. Additionally, this breath hold challenge has been examined as a means to calibrate BOLD signals both spatially and across subjects [18, 19]. Subjects were visually cued to perform a block task of end-inspiration breath holding. Seven blocks of 18 s of free breathing ("rest") with 18 s of visually cued breath holding ("task") were performed. During task, the visual cue instructed subjects to "Take a deep

breath and hold," followed by a counter that indicated progression through the breath hold interval. All subjects were able to complete the task. Subject motion was minimized through a practice session and the use of padding.

BOLD data was acquired using an EPI sequence with an echo time (TE) of 30 ms and a repetition time (TR) of 2 s. Thirty-two slices 4 mm think with a 10% gap between slices were acquired with a field of view of 22 cm and a matrix size of 64. Echo-spacing for the acquisition was 0.4 ms. The positive direction for the phase encode axis was chosen to be posterior-to-anterior, i.e. EPI-up.

3.2.3 Susceptibility Gradient and BOLD Sensitivity Calculation

The unit of field maps is Hz. Gradients of the field maps we obtained simply by calculating the differences of the adjacent pixels in the field map; the unit is Hz/cm. After calculating the gradients, the field maps and gradients maps need to be transformed to a standard space in order to compare them. For image registration, we use the FSL software package provided by the FMRIB group, Functional Magnetic Resonance Imaging of the Brain. The standard image that was used was the template MNI (Montreal Neurological Institute) brain, and registrations of our data to this template were performed using FLIRT (FMRIB's Linear Image Registration Tool) in FSL (FMRIB Software Library).

Effective echo times are calculated by simulating effective k-space trajectories. After including the effects of susceptibility-induced magnetic field gradients, we generated the new k-space trajectory which is possibly shifted and skewed. Then we found a point on the trajectory that has the minimum distance from the origin of the k-space and that would be the effective echo time.

3.3 Result

We focused on the temporal lobe as identified by the MNI structural atlas in FSL [20, 21]. Two regions of interest (ROIs) are created based on the susceptibility-induced magnetic field gradients in the phase encode direction

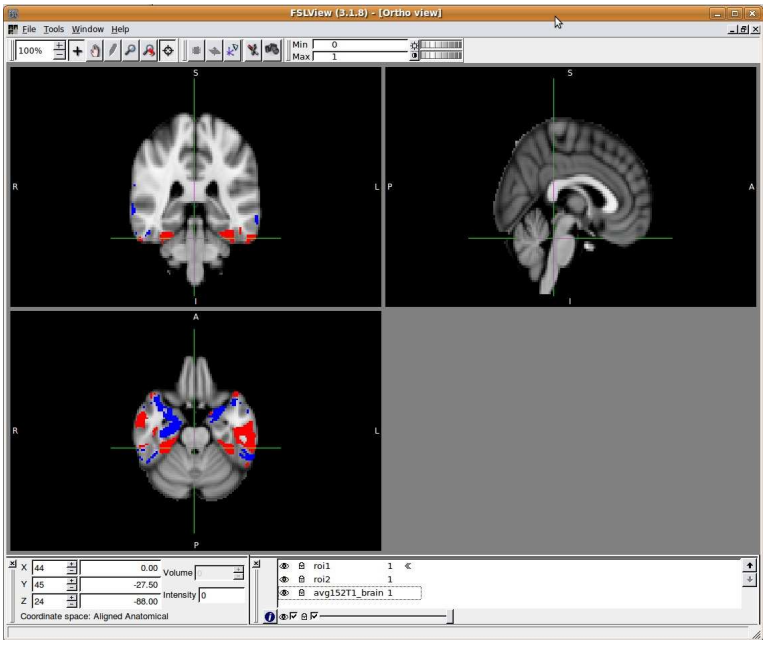

Figure 3.4: ROI1, the red region, is an area where G_Y^{susc} is between -30 Hz/cm and -10 Hz/cm. ROI2, the blue region, is an area where G_Y^{susc} is between 10 Hz/cm and 30 Hz/cm.

(G_Y^{susc}). ROI1 is a region where G_Y^{susc} is between -30 Hz/cm and -10 Hz/cm; this is the red region in Figure 3.4. ROI2 is a region where G_Y^{susc} is between 10 Hz/cm and 30 Hz/cm; this is the blue region in Figure 3.4.

In order to show the validation of calibration, uncalibrated and calibrated PSCs in these ROIs are compared such as in Figure 3.5. First of all, a regression analysis on the PSC of voxels in the two ROIs versus G_Y^{susc} is performed in order to calculate the correlation coefficients. Fisher z-transformation is used to find an average correlation coefficients across subjects:

$$z = \frac{1}{2} \ln \frac{1+r}{1-r} \tag{3.17}$$

After finding the mean of the transformed correlation coefficients, inverse Fisher z-transformation is used:

$$r = \frac{e^{2z}-1}{e^{2z}+1} \tag{3.18}$$

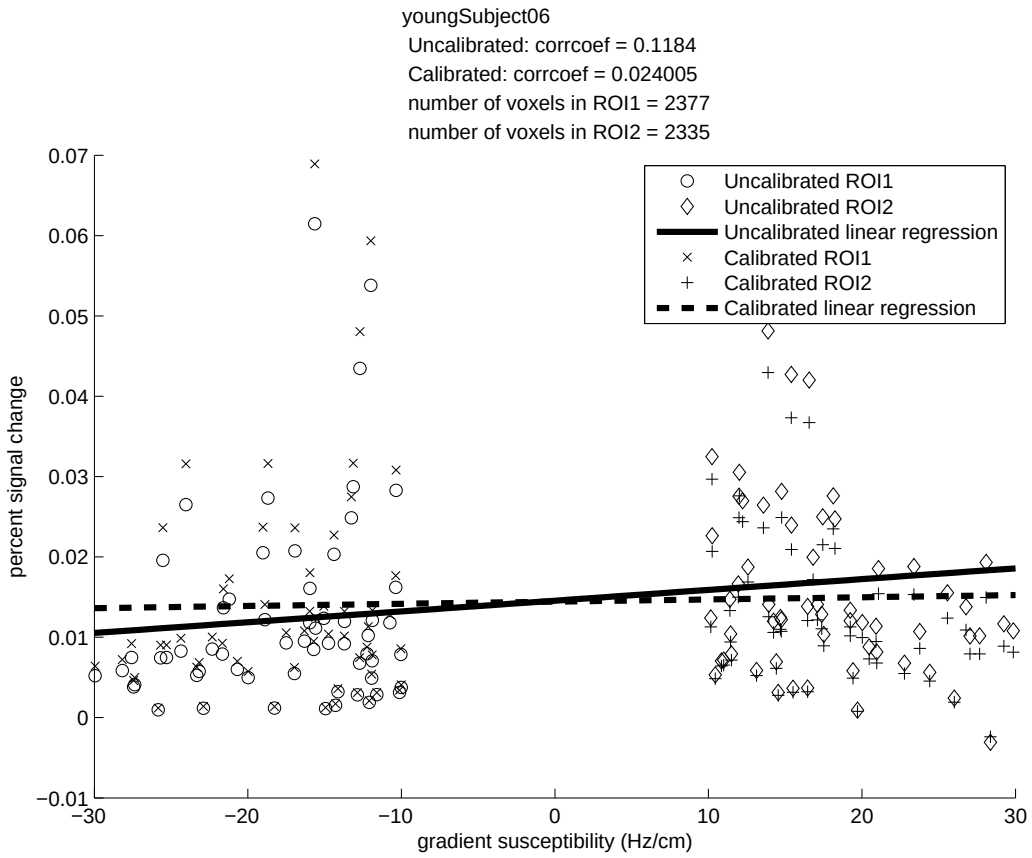

Figure 3.5: Different percent signal changes before and after calibration from a subject.

The average correlation coefficient between signal intensity and susceptibility gradient in the y-direction before the calibration, $R_{uncalibrated}$, is 0.0684 and the average correlation coefficient after the calibration, $R_{calibrated}$, is -0.0028. The decrement of correlation coefficient implies the susceptibility-induced magnetic field gradients have less influence on percent signal change after calibration than before calibration.

The mean of the PSC for each ROI is calculated and an ANOVA analysis is performed. Before the calibration, the PSC of ROI1 = 0.89 $\pm$0.46% and the PSC of ROI2 = 1.13 $\pm$0.56% and the ANOVA analysis gives an F-test = 9.84 and $\eta^2 = 0.05$. After the calibration, the PSC of ROI1 = 0.99 $\pm$0.54% and the PSC of ROI2 = 1.00 $\pm$0.56% and the ANOVA analysis gives an F-test = 0.005 and $\eta^2 = 3 \times 10^{-5}$. Figure 3.6 is the bar chart that contains means and standard deviations of each ROI before and after calibration. The difference of PSCs from the two ROIs was significant before calibration, but

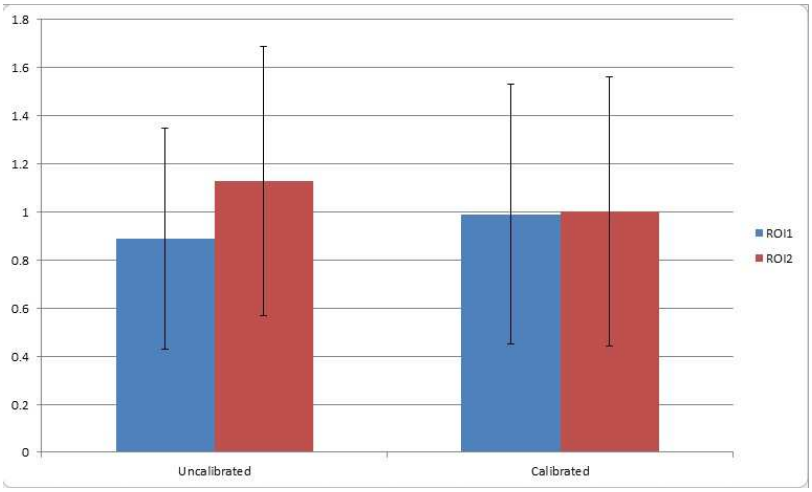

Figure 3.6: Means and standard deviations of each ROI before and after calibration.

it reduced after the calibration.

3.4 Discussion

From past studies such as [3], it has been known that different magnetic susceptibilities can generate artifacts. For example, image distortion, signal loss, and BOLD signal variations can be caused due to macroscopic magnetic susceptibility variations. The region near air/tissue interfaces often has this issue because of different magnetic susceptibilities of air and tissue ($\chi_{tissue} = -9 \times 10^{-6}$ and $\chi_{air} = 0.4 \times 10^{-6}$) [3].

In this study, we focused on how the BOLD signal variations can happen when the k-space trajectory is skewed and shifted and echo time is changed. As shown in Figure 3.1 and Figure 3.2, susceptibility-induced magnetic field gradients can distort the k-space trajectory and the actual echo time will be different from the nominal echo time. In order to correct the distortions

caused by susceptibility-induced magnetic field gradients, we used percent signal change from Equation 3.5 and the calibration function from Equation 3.7, which is already widely being used [15, 16]. We proved that calibration can correct the artifacts.

We also showed that calibration can correct the artifacts from a breath hold task. We defined two regions of interest by susceptibility-induced magnetic field gradients in the phase encode direction. By calibrating percent signal change, we were able to reduce the artifacts. One of the examples is shown in Figure 3.5.

Functional magnetic resonance imaging (fMRI) using blood oxygenation level dependent (BOLD) signals is widely used in many studies. However, the effect of susceptibility-induced magnetic field gradients is usually ignored, although the effect can bring significant sensitivity changes. Percent signal change and calibration function can correct the artifacts simply by using field maps. Percent signal change and calibration function can be used in many applications such as age-related studies, as we will introduce in the next chapter.

CHAPTER 4

GROUP DIFFERENCES IN BOLD SENSITIVITY

4.1 Motivation

The study of how the function of our brain changes with age will enlighten us on how to preserve our mind late into life and will provide information on healthy age-related declines in function versus other pathological changes such as Alzheimer's disease. Much research is being conducted to better understand relationships between fMRI signal increases and their direct relationship to improvement or decrements in behavioral performance across age [22, 23]. Cabeza pointed out that the most powerful studies of the cognitive neuroscience of aging use functional neuroimaging techniques such as functional magnetic resonance imaging (fMRI) [24]. Recently fMRI studies have shown evidence of significant age-related changes in brain function in areas involved with memory, executive control, attention, motor control, and others. Specifically, common findings in the literature demonstrate that aging is associated with changes in magnitude, extent of activation, or laterality. However, magnetic susceptibility can cause spatially-varying BOLD sensitivity in the brain [2, 25]. Therefore, it is necessary to remove these BOLD sensitivity artifacts to have an accurate age-related study. After finding percent signal change ratio from Equation 3.7 and removing the expected variation in the BOLD signal due to susceptibility-induced magnetic field gradients, we are able to examine if there are actual changes in the brain function. In this research, we are going to determine some areas in a brain that have a significant difference in sensitivity with age by comparing the calibration function from Equation 3.7 between a group with young subjects and a group with old subjects.

4.2 Procedures

4.2.1 Acquisition Protocol and Participants

To compare between old and young, two different data sets from previous functional imaging studies are used. The older subject group included twenty-six old adults (59-78 years old, mean age 63.15, 19 females) [26, 27, 28]. The younger subject group consisted of thirty young adults (18-21 years old, mean age 18.8, 18 females) [29, 30]. Subject scans were performed using a Siemens (Erlangen, Germany) Allegra 3 T MRI scanner. For the older group's magnetic field maps, the following are the parameters that are used: TE = 10.00, 12.46 ms, TR = 700 ms, field of view = 22 cm, base resolution = 64, phase resolution = 72, 28 slices 4.00 mm thick, bandwidth = 260.42. The younger group's magnetic field maps were acquired with the same protocol except with the following changes: TR = 1000 ms, 38 slices 3.3 mm thick. We do not expect that these parameter differences would yield different field map measures in our study.

4.2.2 Susceptibility Gradient and BOLD Sensitivity Calculation

The unit of field maps is Hz. Gradients of the field maps are obtained simply by calculating the differences of the adjacent pixels in the field map; the unit is Hz/cm. After calculating the gradients, the field maps and gradients maps need to be transformed to a standard space in order to compare them. For image registration, we use the FSL software package provided by the FMRIB group, Functional Magnetic Resonance Imaging of the Brain. The standard image that was used was the template MNI (Montreal Neurological Institute) brain and registrations of our data to this template were performed using FLIRT (FMRIB's Linear Image Registration Tool) in FSL (FMRIB Software Library).

Table 4.1: Means and standard deviations from the two age groups in several Brodmann's areas (BA - Brodmann's area, μ - mean, σ - standard deviation).

BA	μ_{young}	σ_{young}	μ_{old}	σ_{old}
4	1.03E+00	1.43E-02	1.03E+00	1.72E-02
6	1.01E+00	1.42E-02	1.00E+00	1.38E-02
8	9.91E-01	2.51E-02	9.71E-01	1.76E-02
13	1.01E+00	1.41E-02	9.96E-01	7.41E-03
17	9.77E-01	2.96E-02	1.00E+00	4.51E-02
18	9.47E-01	2.82E-02	9.62E-01	4.54E-02
19	9.63E-01	2.58E-02	9.47E-01	3.78E-02
20	8.84E-01	3.70E-02	8.60E-01	5.13E-02
21	9.72E-01	3.26E-02	9.35E-01	2.25E-02
22	1.00E+00	2.12E-02	9.83E-01	1.24E-02
28	1.04E+00	6.10E-02	9.78E-01	4.62E-02
35	1.00E+00	3.18E-02	9.70E-01	3.54E-02
36	9.71E-01	3.07E-02	9.53E-01	3.77E-02
41	1.02E+00	1.23E-02	1.01E+00	7.31E-03

Table 4.2: Magnitude and effect size of differences of expected activation between the two age groups in several Brodmann's areas (BA - Brodmann's area, PD - percent difference).

BA	-$\log_{10}$p	η^2	ω^2	PD
4	2.97E-01	8.30E-03	-9.88E-03	-2.76E-01
6	1.41E+00	7.68E-02	5.87E-02	7.90E-01
8	2.84E+00	1.73E-01	1.55E-01	1.99E+00
13	3.93E+00	2.42E-01	2.25E-01	1.27E+00
17	1.74E+00	9.92E-02	8.11E-02	-2.51E+00
18	8.89E-01	4.21E-02	2.40E-02	-1.62E+00
19	1.23E+00	6.48E-02	4.66E-02	1.72E+00
20	1.32E+00	7.03E-02	5.21E-02	2.71E+00
21	4.99E+00	3.05E-01	2.88E-01	3.80E+00
22	3.89E+00	2.40E-01	2.23E-01	1.95E+00
28	3.94E+00	2.42E-01	2.25E-01	5.86E+00
35	3.08E+00	1.88E-01	1.71E-01	3.17E+00
36	1.30E+00	6.93E-02	5.12E-02	1.89E+00
41	5.87E+00	3.53E-01	3.37E-01	1.47E+00

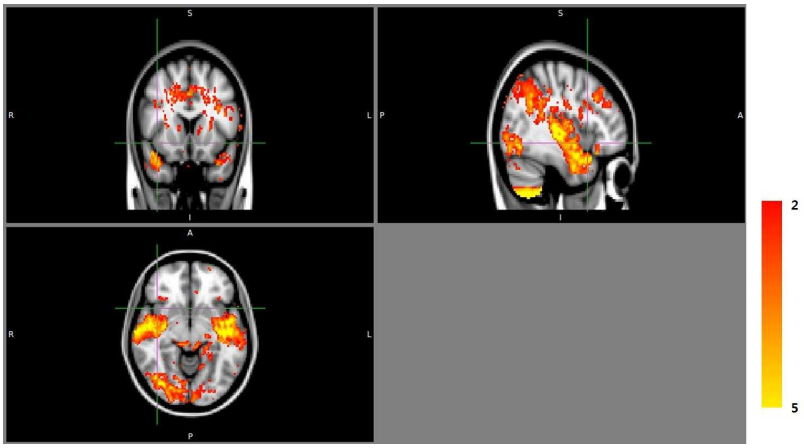

Figure 4.1: Map of $-\log_{10}$(p-value)

4.3 Results

After calculating percent signal change ratio from twenty-six old subjects and thirty young subjects, we performed a voxel-by-voxel t-test in order to find some voxels that have significant differences between these two groups. Red-yellow regions in Figure 4.1 imply voxels whose p-values are between 10^{-2} and 10^{-5}.

Figure 4.2, Table 4.1, and Table 4.2 show some Brodmann areas that have significant differences between young and old adults. In order to extract ROIs in Brodmann areas, the Talairach altas is used which is included with FSL [31, 32, 33]. In each ROI, we extracted all voxels in the ROI and performed voxel-by-voxel ANOVA to find p-values. We also calculated some effect sizes. According to Olejnik and Algina, "an effect-size measure is a standardized index and estimates a parameter that is independent of sample size and quantifies the magnitude of the difference between populations or the relationship between explanatory and response variables" [34].

In this research, we use two effect-sizes, eta-squared (η^2) and omega-

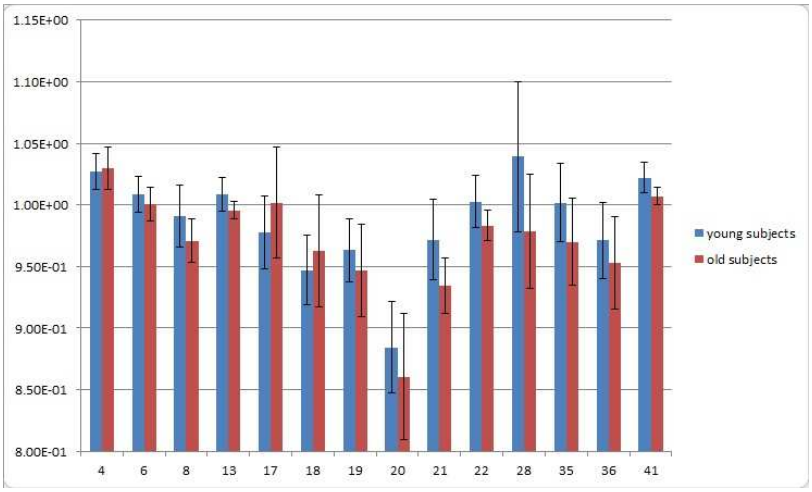

Figure 4.2: Means and standard deviations from the two age groups in several Brodmann's areas. X-axis has Brodmann's areas numbers, and y-axis is calibration function.

squared (ω^2). Eta-squared and omega-squared are defined as following:

$$\eta^2 = \frac{S_{treatment}}{S_{total}} \tag{4.1}$$

$$\omega^2 = \frac{S_{treatment} - df_{treatment} * MS_{error}}{S_{total} + MS_{error}} \tag{4.2}$$

where S symbolizes sum of squares and f symbolizes degrees of freedom.

Percent difference (PD) is defined as

$$PD = \frac{\mu_{young} - \mu_{old}}{\mu_{young}} \times 100 \tag{4.3}$$

where μ symbolizes mean.

4.4 Discussion

Magnetic field variations due to susceptibility differences can result in artifacts of BOLD sensitivity. The variations can affect lots of studies using fMRI such as aging studies. Table 4.1 lists some Brodmann areas which have significant differences of expected BOLD sensitivity ratio between young and old subjects. In order to reduce the artifacts from susceptibility-induced magnetic field gradients, we can divide the percent signal change by the expected BOLD sensitivity ratio.

We are proposing some possible reasons why age-related changes may exist. One of the possible reasons is structural changes due to aging. Previous studies have used voxel-based morphometry (VBM) to assess changes in the overall structure of the brain accompanying age. Birren and Schaie wrote that "VBM uses the intensity value of each voxel in the brain to assign it as gray, white, or cerebrospinal fluid probability and after averaging all participants' brains in the study to a template coordinate space, can calculate group differences at each voxel" [35]. Due to the anatomical changes, the susceptibility-induced magnetic field gradients can also change because the air/tissue interfaces and their relationship to other structures in the brain will change.

Iron concentrations can be also a reason of age-related changes because iron concentration can vary the magnetic field. Age-related results from susceptibility weighted imaging show that iron distributions in the brain can change with age.

Another reason that can result in changes in the distribution of magnetic field is the subject's head orientation. Truong et al. mentioned that the tilted head can significantly reduce or significantly increase the magnetic field gradients depending on which region of the brain is being examined [3], based on how the angle between the air/tissue interfaces and B_0 will be changed. We can get the tilted angle from image registration which calculates the rotation angle from subjects to the template image. The data used in this research show the rotation angles in the x-direction (nod) for old subjects are 0.088 $\pm$0.067 radian and the rotation angles in the x-direction for young subjects are 0.057 $\pm$0.063 radian. The corresponding p-value is 0.087 which means that the rotation angles between old and young subjects are showing a trend towards being different, approaching significance. Generally, people

become stooped as they become older, and this fact might cause this rotation angle difference.

CHAPTER 5

CONCLUSION AND FUTURE WORK

Functional magnetic resonance imaging (fMRI) using blood oxygenation level dependent (BOLD) signals is widely used in many different studies such as aging studies [22, 23, 24]. BOLD is a technique that we can use to find whether a region of interest is active or not as we measure T_2^*-weighted images. Deichmann et al. wrote that variations of echo time can lead into variations of BOLD sensitivity [2]. Different magnetic susceptibilities, which are physical properties that vary between materials, can cause susceptibility-induced magnetic field gradients and they can skew and shift k-space trajectories as Figure 3.1 and Figure 3.2 show. The change of echo time due to shifted and skewed k-space trajectories can bring a significant change of BOLD sensitivity.

In order to reduce the variations of BOLD signals, we suggest percent signal change and calibration function. As we define percent signal change and calibration function, we also conclude that they can correct the artifacts. We also show that the differences of percent signal changes between two ROIs that are created by susceptibility-induced magnetic field gradients in the phase encode direction are reduced after the calibration.

After confirming the validation of percent signal change and the calibration function, we actually applied them in aging studies. Field maps were collected from two different groups, one group with older subjects and the other group with younger subjects. After comparing percent signal change ratio from the two groups, we are able to extract some Brodmann areas from Table 4.1 and Table 4.2 that have significant differences.

Percent signal change and calibration function can be widely used in order to have reliable comparison in fMRI studies. Percent signal change and calibration function can be used to identify some ROIs that are affected by inhomogeneous magnetic fields. Percent signal change and calibration function can also be used to correct the artifacts due to susceptibility-induced

magnetic field gradients. In the future, we will investigate how the choice of pulse sequence impacts BOLD sensitivity. We will try to design pulse sequences that can minimize the sensitivity variations due to magnetic field gradients. Also, we need to research more what factors cause the age-related susceptibility-induced gradient variations. Lastly, percent signal change and calibration function can be used in other group studies where anatomy or physiology differences may result in bulk differences in the magnetic field distribution in the brain.

REFERENCES

[1] P. J. Reber et al., "Correction of off resonance-related distortion in echo-planar imaging using EPI-based field maps," *Magnetic Resonance Imaging*, vol. 39, no. 2, pp. 328–330, Feb. 1998.

[2] R. Deichmann et al., "Compensation of susceptibility-induced BOLD sensitivity losses in echo-planar fMRI imaging," *NeuroImage*, vol. 15, no. 1, pp. 120–135, Jan. 2002.

[3] T.-K. Truong et al., "Three-dimensional numerical simulations of susceptibility-induced magnetic field inhomogeneities in the human head," *Magnetic Resonance Imaging*, vol. 20, no. 10, pp. 759–770, Dec. 2002.

[4] B. P. Sutton et al., "Fast, iterative image reconstruction for MRI in the presence of field inhomogeneities," *Medical Imaging, IEEE Transactions on*, vol. 22, no. 2, pp. 178–188, Feb. 2003.

[5] Z.-P. Liang and P. C. Lauterbur, *Principles of Magnetic Resonance Imaging: A Signal Processing Perspective*. Piscataway, NJ: IEEE Press, 2000.

[6] M. A. Bernstein et al., *Handbook of MRI Pulse Sequences*. Burlington, MA: Elsevier Academic Press, 2004.

[7] G. H. Glover, "Simple analytic spiral k-space algorithm," *Magnetic Resonance in Medicine*, vol. 42, pp. 412–415, Aug. 1999.

[8] N. N. Rao, *Elements of Engineering Electromagnetics*. Upper Saddle River, NJ: Pearson Prentice Hall, 2004.

[9] E. M. Haacke et al., *Magnetic Resonance Imaging : Physical Principles and Sequence Design*. New York: Wiley-Liss, 1999.

[10] R. Deichmann et al., "Optimized EPI for fMRI studies of the orbitofrontal cortex," *NeuroImage*, vol. 19, no. 2, pp. 430–441, June 2003.

[11] C. De Panfilis and C. Schwarzbauer, "Positive or negative blips? the effect of phase encoding scheme on susceptibility-induced signal losses in EPI," *NeuroImage*, vol. 25, no. 1, pp. 112–121, Mar. 2005.

[12] N. Weiskopf et al., "Optimal EPI parameters for reduction of susceptibility-induced BOLD sensitivity losses: A whole-brain analysis at 3 T and 1.5 T," *NeuroImage*, vol. 33, pp. 493–504, Sep. 2006.

[13] N. Weiskopf et al., "Optimized EPI for fMRI studies of the orbitofrontal cortex: Compensation of susceptibility-induced gradients in the readout direction," *Magnetic Resonance Materials in Physics, Biology and Medicine*, vol. 20, no. 1, pp. 39–49, Feb. 2007.

[14] E. Balteau et al., "Improved shimming for fMRI specifically optimizing the local BOLD sensitivity," *NeuroImage*, vol. 49, no. 1, pp. 327–336, Jan. 2010.

[15] M. S. Cohen and R. M. DuBois, "Stability, repeatability, and the expression of signal magnitude in functional magnetic resonance imaging," *Journal of Magnetic Resonance Imaging*, vol. 10, pp. 33–40, Mar. 1999.

[16] M. W. L. Chee et al., "Reproducibility of the word frequency effect: Comparison of signal change and voxel counting," *NeuroImage*, vol. 18, no. 2, pp. 468–482, Feb. 2003.

[17] F. Fera et al., "EPI-BOLD fMRI of human motor cortex at 1.5 T and 3.0 T: Sensitivity dependence on echo time and acquisition bandwidth," *Journal of Magnetic Resonance Imaging*, vol. 19, no. 1, pp. 19–26, Jan. 2004.

[18] C. Chang et al., "Mapping and correction of vascular hemodynamic latency in the BOLD signal," *NeuroImage*, vol. 43, no. 1, pp. 90–102, Oct. 2008.

[19] M. E. Thomason et al., "Calibration of BOLD fMRI using breath holding reduces group variance during a cognitive task," *Human Brain Mapping*, vol. 28, no. 1, pp. 59–68, Jan. 2007.

[20] Collins et al., "Automatic 3-D model-based neuroanatomical segmentation," *Human Brain Mapping*, vol. 3, no. 3, pp. 190–208, 1995.

[21] Mazziotta et al., "A probabilistic atlas and reference system for the human brain: International consortium for brain mapping (ICBM)," *Philosophical Transactions of the Royal Society B Biological Sciences*, vol. 356, no. 1412, pp. 1293–1322, 2001.

[22] J. L. Woodard and M. A. Sugarman, "Functional magnetic resonance imaging in aging and dementia: Detection of age-related cognitive changes and prediction of cognitive decline," *Current Topics in Behavioral Neurosciences*, Sep. 2011.

[23] P. A. Reuter-Lorenz and D. C. Park, "Human neuroscience and the aging mind: A new look at old problems," *The Journals of Gerontology Series B: Psychological Sciences and Social Sciences*, vol. 65B, pp. 405–415, May 2010.

[24] R. Cabeza, "Cognitive neuroscience of aging: Contributions of functional neuroimaging," *Scandinavian Journal of Psychology*, vol. 42, p. 277286, Dec. 2001.

[25] M. L. Gorno-Tempini et al., "Echo time dependence of BOLD contrast and susceptibility artifacts," *NeuroImage*, vol. 15, no. 1, pp. 136–142, Jan. 2002.

[26] K. I. Erickson et al., "Exercise training increases size of hippocampus and improves memory," *Proceedings of the National Academy of Sciences*, vol. 108, pp. 3017–3022, Feb. 2011.

[27] M. W. Voss et al., "Effects of training strategies implemented in a complex videogame on functional connectivity of attentional networks," *NeuroImage*, vol. 59, no. 1, pp. 138–148, Jan. 2012.

[28] R. S. Prakash et al., "Cardiorespiratory fitness and attentional control in the aging brain," *Frontiers in Human Neuroscience*, vol. 4, pp. 1–12, Jan. 2011.

[29] S. L. Warren et al., "Effects of adult attachment and emotional distractors on brain mechanisms of cognitive control," *Psychological Science*, vol. 21, no. 12, pp. 1818–1826, Dec. 2010.

[30] J. M. Spielberg et al., "Trait approach and avoidance motivation: Lateralized neural activity associated with executive function," *NeuroImage*, vol. 54, no. 1, pp. 661–670, Jan. 2011.

[31] Talairach et al., *Co-planar Stereotaxic Atlas of the Human Brain*. New York: Pearson Prentice Hall, 1988.

[32] Lancaster et al., "Bias between MNI and Talairach coordinates analyzed using the ICBM-152 brain template," *Human Brain Mapping*, vol. 28, no. 11, pp. 1194–1205, Nov. 2007.

[33] Lancaster et al., "Automated Talairach atlas labels for functional brain mapping," *Human Brain Mapping*, vol. 10, no. 3, pp. 120–131, July 2000.

[34] S. Olejnik and J. Algina, "Generalized eta and omega squared statistics: Measures of effect size for some common research designs," *Psychological Methods*, vol. 8, no. 4, pp. 434–447, 2003.

[35] J. E. Birren and K. W. Schaie, *Handbook of the Psychology of Aging*. San Diego, CA: Academic Press, 2001.